Aqueous synthesis of core/shell/shell ZnSeS/Cu:ZnS/ZnS quantum dots and their use as a probe for the selective photoluminescent detection of Pb2+ in water

Salima Mabrouk, Hervé Rinnert, Lavinia Balan, Jordane Jasniewski, Ghouti Medjahdi, Rafik Ben Chaabane, Raphaël Schneider

Aqueous synthesis of core/shell/shell ZnSeS/Cu:ZnS/ZnS quantum dots and their use as a probe for the selective photoluminescent detection of Pb^{2+} in water

Salima Mabrouk [a,b], Hervé Rinnert [c], Lavinia Balan [d], Jordane Jasniewski [e], Ghouti Medjahdi [c], Rafik Ben Chaabane [b], Raphaël Schneider [a,*]

[a] Université de Lorraine, CNRS, LRGP, F-54000 Nancy, France

[b] Laboratoire Interfaces et Matériaux Avancés, LIMA, LR011ES55, Faculté des Sciences de Monastir, Avenue de l'environnement, 5019, Tunisie

[c] Université de Lorraine, CNRS, IJL, F-54000 Nancy, France

[d] CEMHTI-UPR 3079 CNRS, Site Haute Température, 1D avenue de la Recherche Scientifique, 45071 Orléans, France

[e] Université de Lorraine, LIBio, F-54000 Nancy, France

* Corresponding author. E-mail address: raphael.schneider@univ-lorraine.fr

Abstract. Water-dispersible core/shell/shell ZnSeS/Cu:ZnS/ZnS quantum dots (QDs) capped with 3-mercaptopropionic acid (3-MPA) were successfully prepared via a one-pot method. The dots are photostable, exhibit a Cu-related photoluminescence (PL) emission located at 500 nm and a PL quantum yield of 21%. The PL of ZnSeS/Cu:ZnS/ZnS QDs was demonstrated to be selectively quenched by Pb^{2+} ions and a method for the rapid and sensitive detection of Pb^{2+} in real water samples was developed. Under the optimized conditions, the PL intensity of ZnSeS/Cu:ZnS/ZnS QDs is almost linearly dependent on the Pb^{2+} concentration in the range of 0.04 to 6 µM and the detection limit is 21 nM in water. Based on PL lifetime and UV-visible absorption measurements, a dynamic quenching mechanism was demonstrated. ZnSeS/Cu:ZnS/ZnS QDs were also demonstrated to be efficient probes for the detection of Pb^{2+} in real water samples. The developed method is rapid, simple and sensitive and demonstrates that ZnSeS/Cu:ZnS/ZnS QDs can be used as non-toxic probes to sense Pb^{2+} ions in aqueous solution.

Keywords: ZnSeS/Cu:ZnS/ZnS QDs; Photoluminescence; Pb^{2+} ions; Dynamic quenching; Sensors.

1. Introduction

Lead ion (Pb^{2+}) is one of the most toxic heavy metal cations and causes severe health problems to humans and plants. In the human body, Pb^{2+} ions may disrupt the DNA transcription process, the nervous system or the respiratory system [1-4]. Pb^{2+} ions may also cause permanent damage to the ecological systems due to their bioaccumulation and non-biodegradation, even at low concentration. Thus, the development of a fast, reliable, sensitive and selective methods for the detection of Pb^{2+} ions in aqueous media is of high importance.

The main analytical tools for the detection of Pb^{2+} include atomic fluorescence spectroscopy [5], atomic absorption spectrometry [6], high performance liquid chromatography coupled with UV-visible detection [7] and electrochemistry [8] but these techniques suffer from sophisticated equipment and long-time analysis. The use of photoluminescent sensors for the detection of Pb^{2+} is a valuable alternative as it is fast, cheap, selective and sensitive [9-11].

Over the past two decades, photoluminescent semiconductor nanocrystals (also called quantum dots, QDs) have been the subject of great interest owing to their unique electronic and optical properties which can be tuned by varying their size, composition or shape or by doping [12-15]. Various QDs or QDs-based assemblies like CdTe [16,17], CdTe associated to gold nanoparticles [18,19], CdSe [20], core/shell CdSe/CdS [21], ZnSe [22], Mn-doped ZnS or ZnSe [23-25], graphene or C-dots [26-29], MoS_2 [30] and Si nanocrystals [31] were demonstrated to be of interest for Pb^{2+} sensing with detection limits up to 0.71 nM. In most of the cases, the detection is based on cation exchange at the surface of the dots or interaction with the capping ligand that induce changes in the optical properties. Noteworthy is that these changes may also occur with other cations present in the aqueous medium which limits the detection of Pb^{2+} in real water samples.

The incorporation of a small amount of a dopant impurity in wide bandgap semiconductors like zinc chalcogenides allows to modify the electronic states into the bandgap which provides to doped-QDs unique advantages such as minimum self-absorption due to a large Stokes shift,

longer excited-state lifetime and high thermal and photostability [32-34]. Recently, the Cu-doping of ZnS and ZnSe QDs has been investigated and it was demonstrated that the relaxation of the exciton occurs *via* the t_2 energy states of Cu^{2+} resulting in an emission in the green region valuable for applications such as bio-imaging, sensing, photocatalysis and light emitting devices [35-48]. Gradient alloyed ZnSeS QDs are well-known to exhibit improved optical properties and higher stability compared to binary ZnS or ZnSe QDs [49-53] but their doping with Cu has only scarcely been investigated [54,55]. Core/shell Cu-doped ZnSeS/ZnS QDs were prepared using the nucleation-doping method in which the Cu dopant is introduced at the earlier stage of the synthesis and thus located in the ZnSeS core [54,55]. The PL emission of these dots is located at 490 nm.

Herein, we report first a one-pot synthesis of 3-mercaptopropionic acid (3-MPA)-capped core/shell/shell ZnSeS/Cu:ZnS/ZnS QDs that show pure and intense Cu-related photoluminescence emission at 500 nm and a PL quantum yield (PL QY) in water of 21% when the dopant is introduced in the first ZnS shell. Next, ZnSeS/Cu:ZnS/ZnS QDs were used as photoluminescent probes for the detection of Pb^{2+} and a selective quenching of the PL emission in the presence of Pb^{2+} was observed. Only weak interference with other metal cations and biomolecules is observed. The detection limits are of 21, 76 and 28 nM in ultrapure water, mineral water and lake water, respectively, indicating that ZnSeS/Cu:ZnS/ZnS QDs are valuable probes for the fast, sensitive and selective detection of Pb^{2+} in real water samples.

2. Experimental section

2.1. Materials

Zinc nitrate hexahydrate $Zn(NO_3)_2 \bullet 6H_2O$ (> 99.0%, Sigma-Aldrich), 3-mercaptopropionic acid (> 99%, Sigma-Aldrich), selenium powder (99.5+%, Sigma-Aldrich), sodium borohydride (99%, Sigma-Aldrich), sodium sulfide nonahydrate $Na_2S \bullet 9H_2O$ (98.0% min, Alfa Aesar) and copper(II) acetate monohydrate $Cu(OAc)_2 \bullet H_2O$ (≥ 99.0 %, Merck) were used for the synthesis of QDs without further purification.

The following reagents were used for detection experiments : sodium chloride (99.9 %, VWR Chemicals), calcium chloride dihydrate (99%, Carlo Erba), chromium(III) nitrate nonahydrate (99%, Acros Organics), manganese(II) chloride tetrahydrate (≥ 99%, Sigma-Aldrich), lithium

chloride anhydrous (≥ 99%, Sigma-Aldrich), mercury(II) nitrate monohydrate (≥ 98.5%, Sigma-Aldrich), iron(III) nitrate nonahydrate (98-101%, Sigma-Aldrich), cadmium nitrate tetrahydrate (98%, Sigma-Aldrich), aluminum nitrate nonahydrate (≥ 98%, Sigma-Aldrich), zinc nitrate hexahydrate (> 99.0%, Sigma-Aldrich), nickel(II) nitrate hexahydrate (99.9%, Sigma-Aldrich), magnesium chloride anhydrous (99%, Alfa Aesar), ammonium iron(II) sulfate hexahydrate (99%, Alfa Aesar), lead(II) nitrate (99%, Alfa Aesar), potassium chloride (>99%, Fluka), chromium(VI) oxide (>99%, Fluka), copper(II) nitrate trihydrate (>99.5%, Merck), cobalt(II) nitrate hexahydrate (>99%, Merck), urea (99.5%, Acros Organics), cholesterol (>99%, Sigma-Aldrich), albumin from chicken egg white (≥90%, Sigma-Aldrich), L-cysteine (L-Cys, ≥ 97%, Sigma-Aldrich), L-histidine (L-His, ≥99%, Fluka), glycin (Gly, 99.1-101%, Riedel-de Haën), D(+) glucose anhydrous (>99.5%, Merck), boric acid (>99.5, Merck), aspartic acid (AA, ≥99%, Sigma-Aldrich) were used as received. All solutions were prepared with deionized water (18.2 MΩ cm). Borate buffered saline (BBS) solution was prepared using a boric acid concentration of 0.1 mM and the final pH was adjusted to 9.

2.2. Synthesis of core/shell/shell ZnSeS/Cu:ZnS/ZnS QDs

A one-pot three-step method was developed for the preparation of ZnSeS/Cu:ZnS/ZnS QDs. In a three- necked flask, $Zn(NO_3)_2$ (0.75 mmol) and 3-MPA (100 µL, 1.147 mmol) are solubilized in 20 mL of ultrapure water at room temperature. The pH of the solution is adjusted to 11 by adding dropwise a 1 M NaOH aqueous solution and oxygen is removed from the reaction medium by bubbling with argon for 30 min. Separately, the NaHSe solution was prepared by reacting 0.215 mmol of Se(0) with 7.93 mmol of $NaBH_4$ in 4 mL of ultra-pure water. The solution becomes colorless after 10 min of stirring under argon. Then, the NaHSe solution is quickly injected to the $Zn(NO_3)_2$ and 3-MPA solution and stirring is maintained for 15 min. Next, $Na_2S.9H_2O$ (0.215 mmol) in 2 mL of water is quickly injected into the mixture and the mixture stirred for 5 min at room temperature. Finally, the reaction mixture was heated at 100°C for 4 h under argon to obtain ZnSeS core QDs.

A Cu-doped ZnS shell was deposited at the surface of ZnSeS cores by simultaneously adding 0.65 mL of a 0.15 M $Zn(NO_3)_2$ solution containing 0.0187 mmol of $Cu(OAc)_2$ and 0.65 mL of a 0.1 M $Na_2S.9H_2O$/0.04 M 3-MPA solution (pH adjusted to 11) using two different syringes. After 1 h, a second ZnS shell was added using the same method. An injection of Zn^{2+} and S^{2-}

precursors is considered to allow the addition of a monolayer to the surface of ZnSeS cores. After cooling to room temperature, the ZnSeS/ZnS:Cu/ZnS QDs were precipitated using ethanol, collected by centrifugation (4000 rpm for 15 min) and washed with ethanol (2 x 20 mL) before use.

2.3. Photostability experiments

The photostability was evaluated by continuously irradiating an aqueous dispersion of ZnSeS/ZnS:Cu/ZnS QDs as well as a solution of fluorescein with a Hg-Xe lamp for 1 h (light intensity of 50 mW/cm^2). The optical properties were monitored by UV-visible and fluorescence spectroscopy.

2.4. Preparation of metal salts, biomolecules and QDs stock solutions

The following metals salts were selected: $Co(NO_3)_2 \bullet 6H_2O$, $Ni(NO_3)_2 \bullet 6H_2O$, $Pb(NO_3)_2$, $Zn(NO_3)_2 \bullet 6H_2O$, $Cu(NO_3)_2 \bullet 3H_2O$, $Al(NO_3)_2 \bullet 9H_2O$, $Fe(NO_3)_2 \bullet 9H_2O$, $Cd(NO_3)_2 \bullet 4H_2O$, $MnCl_2 \bullet 4H_2O$, $Hg(NO_3)_2$, $(NH_4)_2Fe(SO_4)_2 \bullet 6H_2O$, CrO_3, $Cr(NO_3)_3 \bullet 9H_2O$, KCl, NaCl, $MgCl_2$, $CaCl_2$ and LiCl. Stock solutions of these salts were prepared with a 1 mM concentration and then diluted to the desired concentration.

The interference of the following biomolecules was also investigated: L-Cysteine (L-Cys), L-Histidine (L-His), Glycine (Gly), Aspartic acid (Asp), glucose and urea stock solutions were prepared with a 1 mM concentration. The cholesterol solution was prepared by dispersing 0.5 mg of this compound into 100 mL of deionized water. The albumin solution was prepared based on its concentration in the blood (35 mg/mL) and then diluted to the desired concentration.

The stock solution of ZnSeS/ZnS:Cu/ZnS QDs was prepared with a concentration of 0.2 mg/mL.

2.5. PL response of ZnSeS/ZnS:Cu/ZnS QDs towards metal cations

50 µL of the different salts at a concentration of 0.2 mM were added to 2 mL of ZnSeS/ZnS:Cu/ZnS QDs at a concentration of 0.2 mg/mL. The mixture was shacked and the PL was measured after 5 min incubation using an excitation wavelength of 350 nm.

2.6. Spectrofluorometric detection of Pb^{2+} ions using ZnSeS/ZnS:Cu/ZnS QDs

The PL spectrum of the QDs aqueous dispersion (2 mL) was recorded at room temperature with an excitation wavelength of 350 nm. Then, the Pb^{2+} ions solution was introduced as aliquots of increasing concentration (from 0-20 µM) 5 min before recording the PL emission spectra. The same conditions were used for steady state and time-resolved PL measurements.

2.7. Influence of biomolecules on the Pb^{2+} detection

First, 200 µL of the QDs dispersion (concentration of 0.2 mg/mL) are added to 2 mL of the various biomolecule solutions. An aliquot of 50 µL of the Pb^{2+} solution (concentration 0.2 mM) is then added. The mixture is shacked and the fluorescence was measured after 5 min using an excitation wavelength of 350 nm.

2.8. Analysis of real water samples

Mineral water from local market and lake water (filtered through a 0.2 µm membrane) were also used to evaluate the reliability of the Pb^{2+} detection method. The QDs and Pb^{2+} stock solutions were prepared in these water samples. Next, the Pb^{2+} ions solution was introduced as aliquots of increasing concentration (from 0-20 µM) 5 min before recording the PL spectra.

2.9. Characterization

Transmission electron microscopy (TEM) and high-resolution (HR-TEM) measurements were performed on a Philips CM200 instrument operating at 200 kV. The powder X-ray diffraction (XRD) patterns were recorded using a Panalytical X'Pert Pro MPD diffractometer using Cu Kα radiation (λ = 0.15418 nm). The dried samples were placed on a silicon zero-background sample holder and the XRD patterns were recorded at room temperature. The surface states and chemical composition of the QDs were determined by X-ray photoelectron spectroscopy (XPS) using Gammadata Scienta SES 200-2 spectrometer. Hydrodynamic QDs sizes, polydispersity indexes (PDI), and Zeta potential measurements were determined by dynamic

light scattering (DLS) on a Zetasizer Nano ZS (Malvern Panalytical, UK) equipped with a He/Ne ion laser at λ = 532 nm in a backscattering configuration with a measurement angle of 173 °. Experiments were performed at 25 °C with capillary disposable cuvette DTS1070.

The Fourier transform infrared (FT-IR) spectra were recorded on a Brucker ALPHA spectrometer. UV-visible absorption spectra were obtained with a Thermo Scientific Evolution 220 UV-visible spectrophotometer. Photoluminescence (PL) emission spectra were recorded on a Horiba Fluoromax-4 Jobin Yvon spectrofluorometer. PL spectra were corrected and PL QYs were determined relative to fluorescein (PL QY = 95% in a 0.1 M NaOH solution). For the time resolved photoluminescence (TR-PL) experiments, the QDs were pumped by the 355 nm line of a frequency-tripled YAG (yttrium aluminium garnet):Nd laser. The laser pulse frequency, energy and duration were typically equal to 10 Hz, 50 µJ and 10 ns, respectively. The PL signal was analysed by a monochromator equipped with a 600 grooves/mm grating and by a photomultiplier tube cooled at 190 K. The rise time of the detector is equal to around 3 ns.

3. Results and discussion

3.1. QDs synthesis and optical properties

Core/shell/shell ZnSeS/Cu:ZnS/ZnS QDs were prepared using a one-pot aqueous phase process described in Scheme 1. Preliminary experiments not described here showed that QDs exhibiting the highest PL QY for the Cu-related emission were obtained by introducing the Cu dopant in the first ZnS shell covering the ZnSeS core. After the core synthesis, a mixture of $Zn(NO_3)_2$, $Cu(OAc)_2$ and Na_2S was injected to create the Cu:ZnS shell at the surface of the ZnSeS core. Noteworthy is that the Cu^{2+} precursor is reduced into Cu^{+} during that step as demonstrated by XPS (*vide infra*) and electron spin resonance (data not shown), which agrees with previous reports [40]. Finally, a ZnS shell is deposited at the periphery of ZnSeS/Cu:ZnS QDs to protect the dots from the environment and improve the PL QY.

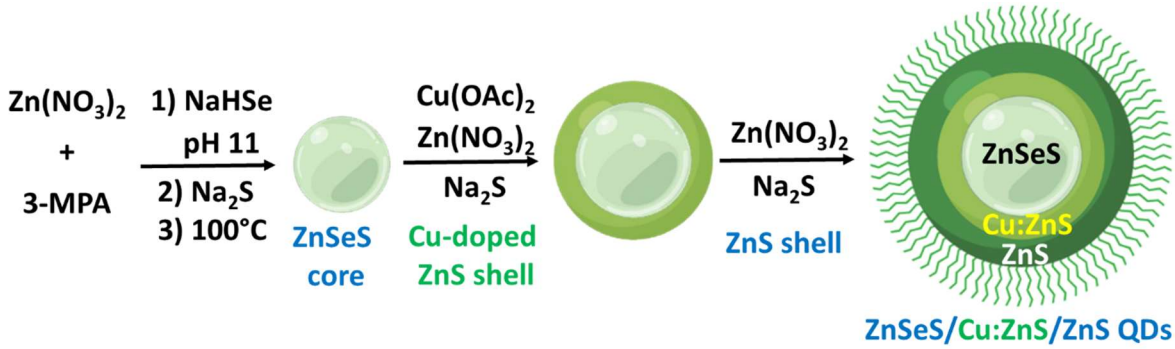

Scheme 1. Schematic representation of the synthesis of ZnSeS/Cu:ZnS/ZnS QDs.

UV-visible absorption spectra of ZnSeS, ZnSeS/Cu:ZnS and ZnSeS/Cu:ZnS/ZnS QDs exhibit a poorly resolved shape, indicating that the Cu doping has no influence on the electronic properties of the ZnSeS/ZnS host material (Fig. 1a). The absorption edges slightly shift to longer wavelength after introduction of the Cu:ZnS and of the ZnS shells, which confirms the size increase of the dots.

The ZnSeS core exhibits an emission centered at 480 nm originating from donor-acceptor states (Fig. 1b). This emission is not shifted after capping the ZnSeS core with one or two ZnS shells (Fig. S1). However, after incorporation of Cu^{+} into the first ZnS shell, the emission changes from blue to green and the PL maximum is shifted to 487 nm, which is the characteristic PL emission of Cu^{2+} [56-58]. A further shift to 500 nm is observed after the introduction of the second ZnS shell at the surface of the Cu-doped ZnS shell. The inset of Fig. 1b shows a photograph taken under UV light illumination of ZnSeS and ZnSeS/Cu:ZnS/ZnS QDs which confirms that the PL emission changes from blue to green after introduction of the Cu:ZnS and ZnS shells at the surface of the ZnSeS core. The PL QYs of ZnSeS, ZnSeS/Cu:ZnS and ZnSeS/Cu:ZnS/ZnS QDs are of 10, 17 and 21%. Based on data available in the literature [56-58], the following mechanism can be proposed for the PL emission of ZnSeS/Cu:ZnS/ZnS. After excitation of the host, Cu^{+} binds with the hole in the valence band (VB) producing a transient Cu^{2+} acceptor state. Next, the electron promoted from the conduction band (CB) to a shallow trap state recombines with the hole-trapped *d* state of Cu^{2+} resulting in the formation of Cu^{+} and to the green emission at 500 nm (Fig. 1c).

The photostability of ZnSeS/Cu:ZnS/ZnS QDs is crucial for their practical applications and was evaluated under the continuous irradiation of a Hg-Xe lamp and compared to that of fluorescein. As can be seen from Fig. 1d, a ca. 1.25-fold increase of the PL intensity of the dots

is observed during the illumination likely due to the decomposition of the 3-MPA ligand and the concomitant release of S^{2-} ions that associate with surface Zn^{2+} atoms to create an extra ZnS shell (see Fig. S2 for UV-visible and PL emission spectra during the irradiation). The overcoating with a ZnS shell further protects the Cu^{+} dopant thus avoiding the photobleaching of the Cu-related emission during the irradiation. Under identical excitation conditions, an almost complete disappearance of the PL of fluorescein is observed after 45 min, which demonstrates the high photostability of ZnSeS/Cu:ZnS/ZnS QDs compared to the organic dye.

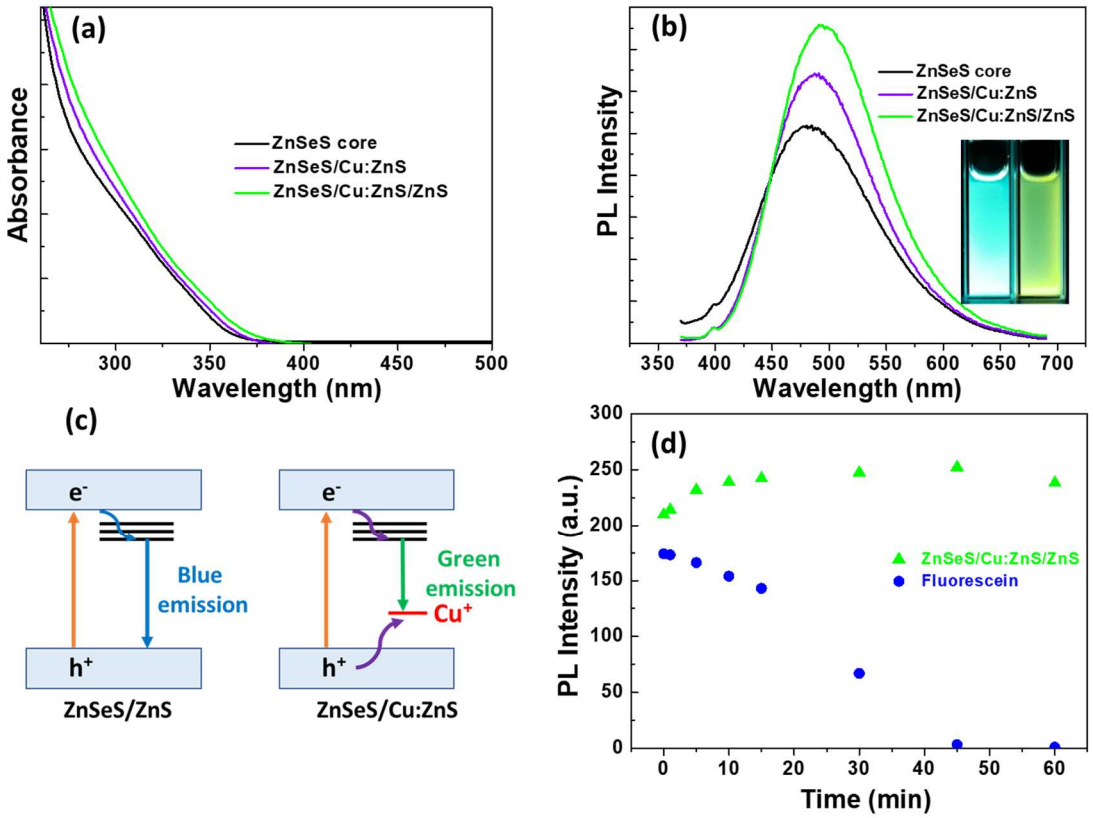

Fig. 1. (a) UV-visible absorption spectra and (b) PL emission spectra of the ZnSeS, ZnSeS/Cu:ZnS and ZnSeS/Cu:ZnS/ZnS QDs (λ_{ex} = 350 nm). The inset of (b) is a digital photograph taken under UV light illumination of ZnSeS and ZnSeS/Cu:ZnS/ZnS QDs. (c) PL emission mechanism and (d) photostability of ZnSeS/Cu:ZnS/ZnS QDs and of fluorescein under the continuous irradiation of a Hg-Xe lamp (intensity of 50 mW/cm^2).

3.2. QDs structure and morphology

Representative HR-TEM images of ZnSeS/Cu:ZnS and ZnSeS/Cu:ZnS/ZnS QDs indicate that the nanocrystals are well dispersed and exhibit a nearly spherical shape (Fig. 2a and 2b, respectively). The inset of Fig. 2b shows that the distance between the adjacent lattice fringes is ca. 0.31 nm, value consistent with the (111) diffraction planes of cubic zinc blende ZnSe (0.327 nm) and ZnS (0.312 nm). The selected area electron diffraction pattern (SAED) shows three concentric rings corresponding to the (111), (220) and (311) planes of the cubic zinc blende structure (insets of Fig. 2a and Fig. 2b). The structure of the dots was further confirmed by XRD (Fig. 2c). The XRD patterns of undoped and Cu-doped ZnSeS/ZnS/ZnS QDs exhibit three peaks located at 28.33, 47.37 and 55.87° corresponding to the (111), (220) and (311) reflecting planes, further confirming that the dots have a cubic zinc blende crystalline structure (JCPSC card No 00-065-0723). The Cu doping doesn't affect the crystalline structure of ZnSeS/ZnS/ZnS QDs. The positions of the diffraction peaks are located between those of cubic zinc blende ZnS and ZnSe, indicating that the alloyed ZnSeS core was successfully prepared. The XRD patterns of Cu:ZnSeS and Cu:ZnSeS/ZnS QDs fit well with that of the host with a $ZnSe_{0.5}S_{0.5}$ composition (see Fig. S3 for the experimental and calculated data) indicating that both Se^{2-} and S^{2-} incorporate similarly in the crystal lattice. The average sizes of ZnSeS/Cu:ZnS and ZnSeS/Cu:ZnS/ZnS QDs are of 1.4 ± 0.5 nm and 1.8 ± 0.5 nm, which confirms that a ZnS shell was deposited at the periphery of ZnSeS/Cu:ZnS/ZnS QDs using the synthetic methodology developed. Moreover, the average diameter of ZnSeS/Cu:ZnS/ZnS QDs determined using the Scherrer equation (2.2 nm) agrees well with TEM measurements (1.8 ± 0.5 nm) (Fig. 2d). Their hydrodynamic diameter was determined by DLS and is of 20.6 ± 2 nm (Fig. 2e), value significantly higher than that determined by TEM and suggesting an association between the QDs in aqueous solution despite of their highly negative Zeta potential (-76 mV) (Fig. 2f).

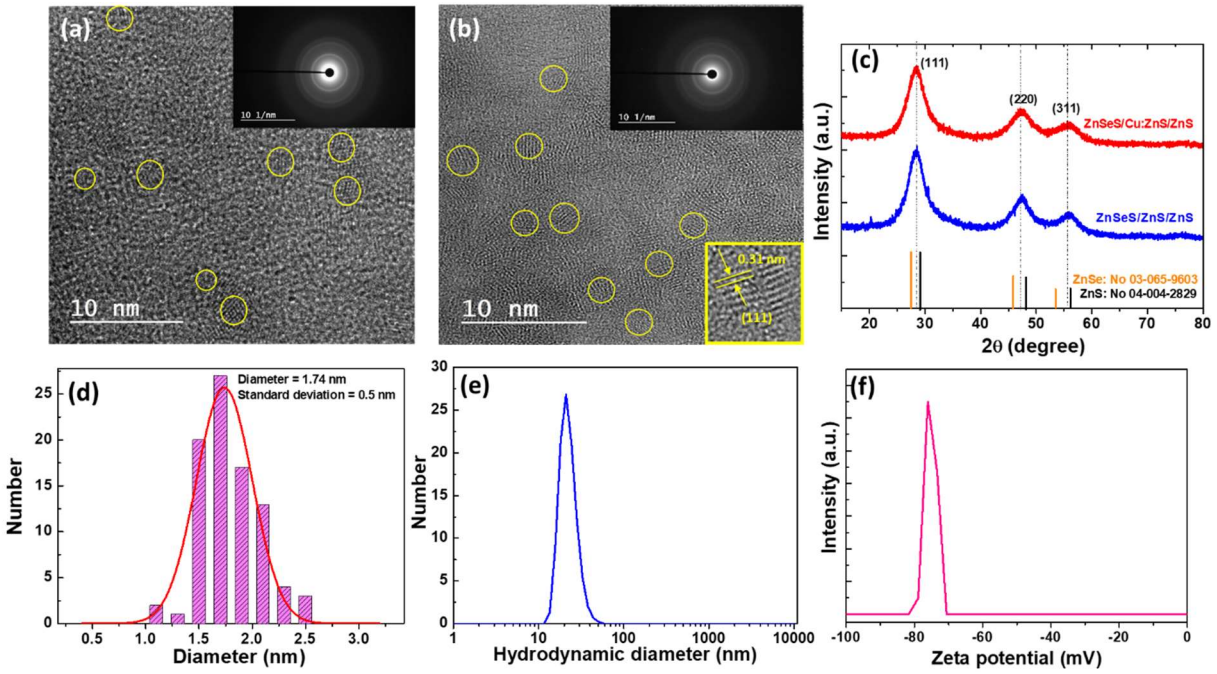

Fig. 2. HR-TEM images of (a) ZnSeS/Cu:ZnS and (b) ZnSeS/Cu:ZnS/ZnS QDs, (c) XRD patterns of undoped and Cu-doped ZnSeS/ZnS/ZnS QDs, (d) the size distribution of ZnSeS/Cu:ZnS/ZnS QDs determined by TEM, (e) their hydrodynamic diameter and (f) their Zeta potential.

The composition of ZnSeS/Cu:ZnS/ZnS QDs was further investigated by FT-IR (Fig. S4). Pure 3-MPA shows a strong signal at 1699 cm^{-1} corresponding to the C=O stretching of the carboxylic acid function and weaker peaks at 2570 and 2659 cm^{-1} corresponding to the stretching of the S-H function and to the carboxylic acid dimer. The thiol signals disappear after the synthesis of the dots due to the covalent bond formed between surface Zn atoms and S. The asymmetric and symmetric stretching of the carboxylate function can be observed at 1556 and 1394 cm^{-1}, respectively, which further confirms that the dots are capped with 3-MPA.

The composition and the chemical state of the elements of ZnSeS/Cu:ZnS/ZnS QDs were further studied by XPS. The XPS survey spectrum shows only the presence of Zn, Se, S, Cu, C, O and Na elements which confirms the purity of the nanocrystals prepared (Fig. S5). The signal of Zn $2p_{3/2}$ is located at 1021.52 eV which is characteristic of Zn(+2) (Fig. 3a) [59]. The Se 3d peak can be deconvoluted into two components located at 53.79 and 54.64 eV corresponding to Se $3d_{5/2}$ and Se $3d_{3/2}$, respectively (Fig. 3b). The energy splitting is of 0.85 eV and confirms the Se(-2) chemical state. The signal of S is more complex as this element is present in the inorganic core of the dots and in the 3-MPA capping ligand (Fig. 3c). The peaks at 161.59 and 162.79 eV correspond to S $2p_{3/2}$ and S $2p_{1/2}$ coordinated to Zn(+2) while the signals at 163.50

and 164.70 eV can be attributed to S $2p_{3/2}$ and S $2p_{1/2}$ of the thiolate ligand. It should also be noted that the Cu $2p_{3/2}$ peak appears at 932.34 eV, which is characteristic of Cu(+1) [60], indicating that the Cu(+2) precursor is likely reduced into Cu(+1) by sulfide S^{2-} anions during the deposition of the Cu-doped ZnS shell at the surface of the ZnSeS core (Fig. 3d).

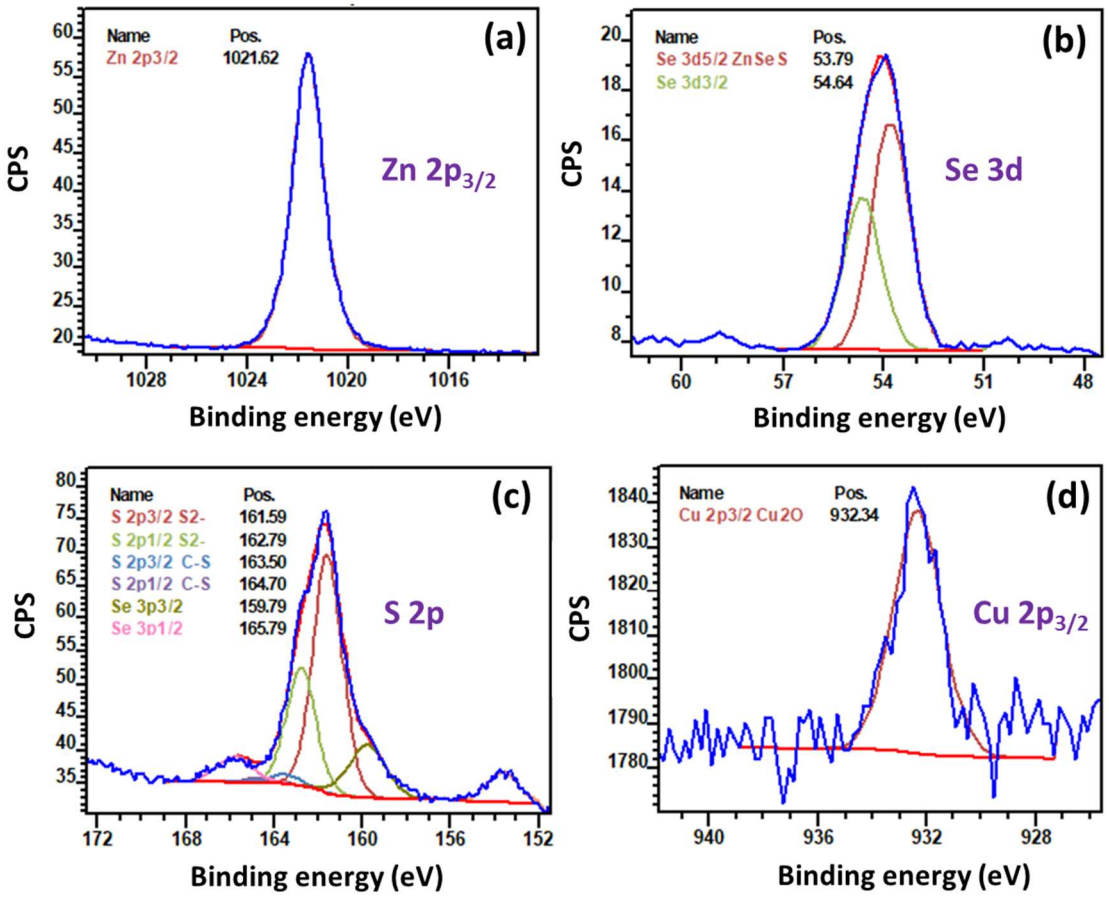

Fig. 3. High resolution XPS spectra of (a) Zn $2p_{3/2}$, (b) Se 3d, (c) S 2p and (d) Cu $2p_{3/2}$.

3.3. Pb^{2+} detection in water and real samples

QDs are well known to interact with some metal cations via surface adsorption, electron transfer or energy transfer which results in PL quenching or enhancement [61]. When Pb^{2+} ions were added to ZnSeS/Cu:ZnS/ZnS QDs, a strong PL decrease was immediately observed. To determine the optimal conditions for the detection of Pb^{2+} in aqueous solution, the influence of the QD structure was first studied. ZnSeS, ZnSeS/Cu:ZnS and ZnSeS/Cu:ZnS/ZnS QDs were exposed to the same amount of Pb^{2+} and the I/I_0 values were determined (I_0 and I corresponding to the PL intensity of ZnSeS/Cu:ZnS/ZnS QDs in the absence and in the presence

of Pb^{2+} ions, respectively). Fig. S6 shows that ZnSeS/Cu:ZnS/ZnS QDs were the most sensitive to Pb^{2+} while the quenching is the less pronounced for undoped ZnSeS/ZnS/ZnS QDs. The increase of the distance between the Cu photoactive center and the surface of the QD, appears to favor the PL quenching (*vide infra*).

Next, the influence of the pH on the PL quenching of the dots was first investigated. QDs capped with small thioacids like 3-MPA exhibit the highest PL intensity at pH values ranging from 5 to 11. Below pH 5, the carboxylate group of the MPA ligand is protonated and QDs precipitate. Above pH 11, hydroxide ions attack Zn^{2+} cations at the surface of the dots to form $Zn(OH)_2$ followed by QDs decomposition. As shown in Fig. S7, the highest I_0/I values obtained after adding Pb^{2+} were obtained for pH values ranging from 7 to 10. Thus, a neutral pH was used in further experiments.

We also investigated the influence of the incubation time after addition of Pb^{2+} on the PL quenching of the dots. Fig. S8 shows that the quenching occurs immediately after making contact between ZnSeS/Cu:ZnS/ZnS QDs and Pb^{2+} and that the PL intensity remains almost unchanged during the 6 min of the experiment. In the follow-up experiments, an incubation time of 5 min was arbitrarily used.

Under these optimal conditions, ZnSeS/Cu:ZnS/ZnS QDs were used for the quantitative detection of Pb^{2+}. As presented in Fig. 4a, the PL intensity of the dots markedly decreases with the increase of the Pb^{2+} concentration from 0.04 to 20 µM. This decrease is accompanied by a blue-shift of the PL maximum from 500 to 488 nm. Fig. 4b shows a linear correlation between I_0/I values and the concentration of Pb^{2+} between 0.04 and 6 µM. The linear regression equation is Y = 2.255X + 0.820 (R^2 = 0.997) where Y is the I_0/I value and X is the Pb^{2+} concentration. The limit of detection (LOD) was determined according to 3σ/k where σ is the standard deviation obtained and k is the slope of the calibration curve and was found to be of 21 nM. A list a QDs developed for Pb^{2+} detection and their LODs are given in Table S1. This data shows that ZnSeS/Cu:ZnS/ZnS QDs have excellent performance for Pb^{2+} sensing.

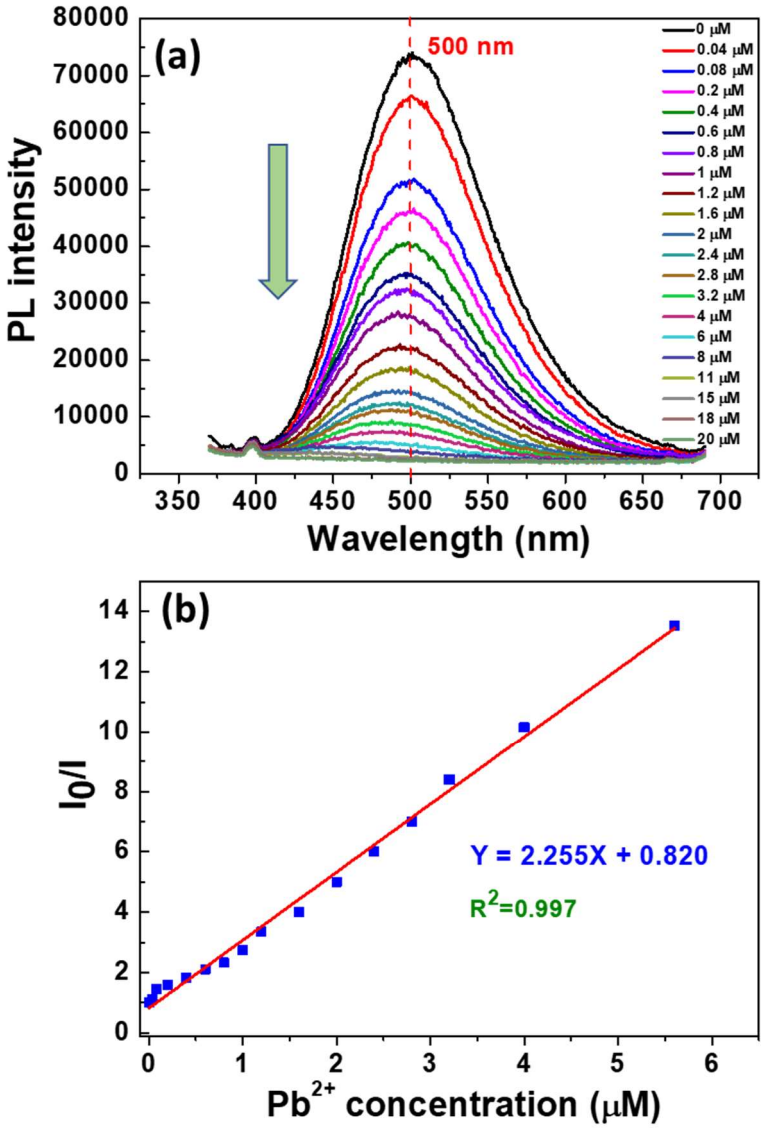

Fig. 4. (a) PL emission spectra of ZnSeS/Cu:ZnS/ZnS QDs dispersed in water upon addition of various concentrations of Pb^{2+}, (b) the linear correlation of I_0/I vs the concentration of Pb^{2+} in the range 0.04-6 µM.

Fig. 5a shows that the PL intensity of ZnSeS/Cu:ZnS/ZnS QDs is almost insensitive to many cations (Al^{3+}, Ca^{2+}, Cr^{6+}, Cr^{3+}, Cu^{2+}, Fe^{2+}, Fe^{3+}, K^{+}, Li^{+}, Mg^{2+}, Mn^{2+}, Na^{+}, Ni^{2+} and Zn^{2+}) used at the same concentration than Pb^{2+}. A decrease of ca. 10% of the PL intensity was observed in the presence of Cd^{2+} and Co^{2+} and of ca. 30% in the presence of Hg^{2+}, indicating that the ZnSeS/Cu:ZnS/ZnS probes allow to discriminate Pb^{2+} from many other metal cations. Fig. 5b is a photograph taken under UV light illumination of ZnSeS/Cu:ZnS/ZnS QDs dispersions after

the addition of the metal cations and shows that the presence of Pb^{2+} can be distinguished by the naked eye as only this cation can effectively quench the PL.

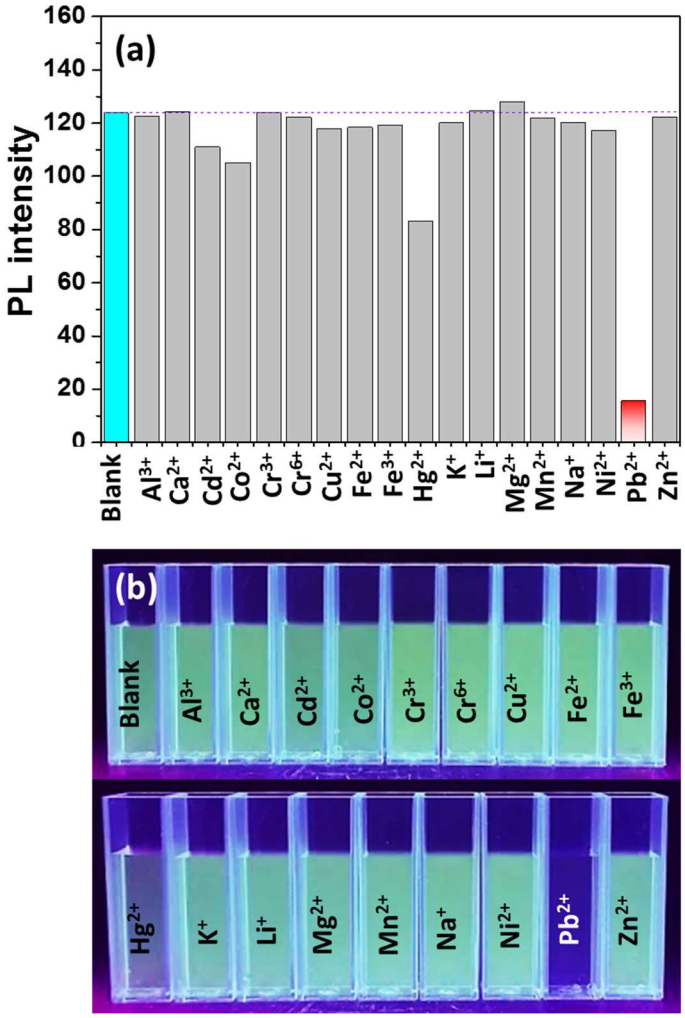

Fig. 5. (a) Sensitivity of ZnSeS/Cu:ZnS/ZnS QDs towards various metal cations, (b) photograph taken under UV light illumination of ZnSeS/Cu:ZnS/ZnS QDs dispersion after addition of the metal cations.

The presence of coexisting cations (Ca^{2+}, Cr^{3+}, Cr^{6+}, Cu^{2+}, Fe^{2+}, Fe^{3+}, K^{+}, Li^{+}, Mg^{2+}, Mn^{2+}, Na^{+} and Zn^{2+} used at 10 µM concentration) did not yield significant interference within the margin of error allowed (Fig. 6a). Similar results were obtained in a 0.1 M BBS, in the presence of various aminoacids (Gly, Lys, His, Asp used at a 1 mM concentration) and biological relevant molecules such as cholesterol, glucose, albumin and urea (Fig. 6b). These results further show that the detection of Pb^{2+} using ZnSeS/Cu:ZnS/ZnS QDs is sensitive and selective.

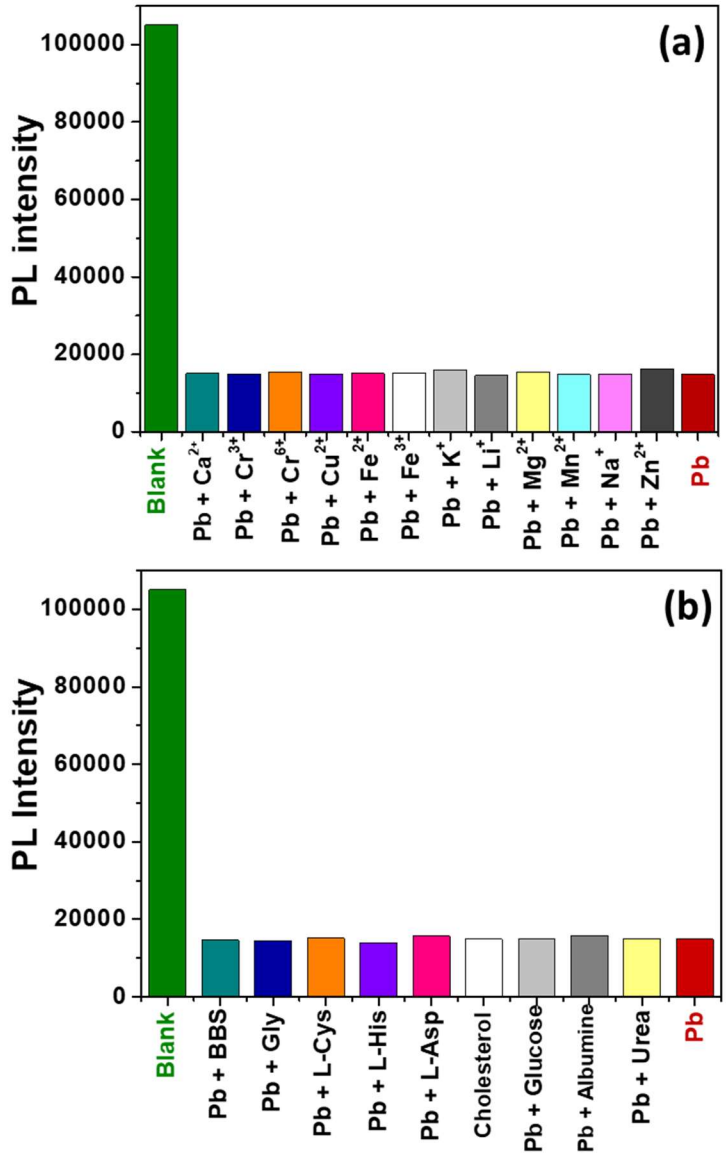

Fig. 6. Selectivity of the ZnSeS/Cu:ZnS/ZnS QDs for the detection of Pb^{2+} in the presence of (a) various metal cations (all cations were used at a 10 µM concentration) and (b) in 0.1 M BBS, in the presence of aminoacids used a concentration of 1 mM and various biological relevant molecules (urea and glucose at a concentration of 1 mM, cholesterol at 0.05 mg/L and albumin at 0.85 mg/mL).

The detection of Pb^{2+} in real water samples was also investigated. No Pb^{2+} ions were detected in mineral and lake water used for these experiments. ZnSeS/Cu:ZnS/ZnS QDs were dispersed in these water samples at a concentration of 0.2 mg/mL and the PL response of the dots to Pb^{2+} was monitored as previously (Fig. 7a,b). As can be seen on Fig. 7a, the PL quenching of the dots in mineral water is very similar to that observed in ultrapure water and a gradual

decrease of the PL intensity is observed with the increase of the Pb^{2+} concentration from 0 to 20 µM. This decrease is accompanied by a shift of the PL emission wavelength from 500 to 486 nm. As previously, a good linear correlation between I_0/I values and the concentration of Pb^{2+} is observed between 0.04 and 6 µM and the LOD was determined to be 76 nM (Fig. 7c). In lake water, a marked shift of the PL emission from 495 to 426 nm is observed upon addition of Pb^{2+} and the calculated LOD is of 28 nM (Fig. 7d). These differences in LOD values are related to the ionic strength of aqueous media (mineral water contains Ca^{2+}, Mg^{2+}, Na^{+}, SO_4^{2-}, NO_3^{-} and HCO_3^{-} ions) and to the presence of organic molecules in lake water and are in good agreement with previous reports [25, 62]. These results demonstrate that ZnSeS/Cu:ZnS/ZnS QDs are reliable and sensitive probes for the detection of Pb^{2+} in real water samples.

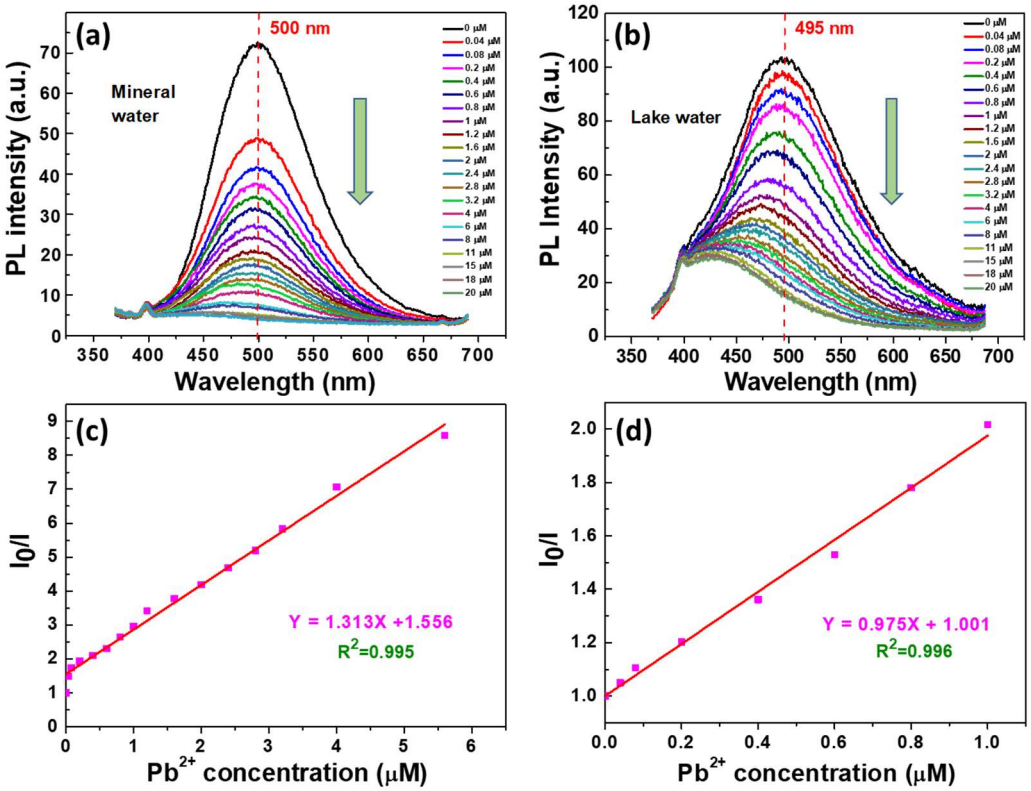

Fig. 7. PL emission spectra of ZnSeS/Cu:ZnS/ZnS QDs dispersed in (a) mineral water and (b) lake water upon addition of various concentrations of Pb^{2+}, (c) and (d) are the corresponding linear correlations of I_0/I vs the concentration of Pb^{2+} in the range 0.04-6 and 0.04-1 µM, respectively.

3.4. Quenching mechanism

The PL quenching may originate either from static or dynamic interactions of the quencher with the QDs. Numerous interactions including complex formation at the ground state, interaction at the excited state, electron transfer or energy transfer may be involved in the quenching [61]. As the PL intensity of ZnSeS/Cu:ZnS/ZnS QDs is quenched upon addition of Pb^{2+} ions, the PL quenching mechanism was further investigated by UV-visible spectroscopy and time-resolved PL measurements.

As can be seen on Fig. S9, no shift of the UV-visible absorption of ZnSeS/Cu:ZnS/ZnS QDs is observed upon addition of Pb^{2+} indicating that Pb^{2+} ions are not incorporated in the nanocrystals. This suggests a collisional (dynamic) quenching mechanism affecting the excited states of the dots. A static quenching would perturb the absorption spectrum of the photoluminescent probe.

The quenching mechanism was further studied by measuring the PL lifetime of the dots which remains constant in a static quenching process but markedly decreases in a dynamic quenching process. Fig. 8 shows the PL decay profiles of ZnSeS/Cu:ZnS/ZnS QDs in the absence of Pb^{2+} and when increasing the concentration of Pb^{2+} from 1 to 8 µM. The PL decays were best fitted using a tri-exponential function with the equation function $I(t) = A_1 \exp(-t/\tau_1) + A_2 \exp(-t/\tau_2) + A_3 \exp(-t/\tau_3)$, where τ_1, τ_2 and τ_3 are the time constants of the PL and A_1, A_2 and A_3 the amplitudes of the components. The average lifetime τ_{av} was determined using the formula $\tau_{av} = (A_1\tau_1 + A_2\tau_2 + A_3\tau_3)/(A_1 + A_2 + A_3)$. The time constants and the amplitudes are listed in Table 1. Due to the presence of Cu *d*-states, the PL lifetime of ZnSeS/Cu:ZnS/ZnS QDs is higher than that of conventional binary QDs and is of ca. 0.186 µs, value in good accordance with those determined for Cu-doped QDs and confirms that the emission mainly originates from the Cu dopant transition and not from surface states or excitonic recombination [63,64]. The short lifetime of 0.033 µs is linked to surface defect states while the two longer PL decays may be associated either to the Cu-related emission or to intrinsic defects located within the bandgap (electron transition from donor to acceptor states like Zn vacancies and S or Se dangling bonds) as previously observed for Cu-doped ZnS nanocrystals [65]. The two latter decays have very close values and it is not possible for us to affect them in the current state of our knowledge.

As can be seen from the results described in Table 1, a decrease of τ_1, τ_2 and τ_3 is observed with the increase of the Pb^{2+} concentration from 1 to 8 µM (by 29, 34 and 41% for τ_1, τ_2 and τ_3, respectively), which yields a decrease of τ_{av} from 0.186 to 0.0789 µs (Fig. S10).

The decrease of the PL lifetime of ZnSeS/Cu:ZnS/ZnS QDs with the increase of the Pb^{2+} concentration from 0 to 0.8 µM follows the Stern-Volmer (S-V) relation:

$I_0/I = \tau_0/\tau = K_{S\text{-}V}[Pb^{2+}] + 1$

where τ_0 and τ are the PL lifetimes of ZnSeS/Cu:ZnS/ZnS QDs in the absence and in the presence of Pb^{2+} ions, respectively. The $K_{S\text{-}V}$ value was determined from the linear S-V plot and is 0.840 μM^{-1}. The quenching constant rate Kq, calculated using the equation $K_{S\text{-}V} = Kq\tau_0$, is 4.51 $M^{-1}s^{-1}$.

Heavy metals ions like Pb^{2+} have a strong affinity for thiol, and to a lesser extent carboxylate functions, the 3-MPA ligand may be partly removed from the surface of the dots upon binding with Pb^{2+} [66]. The formation of the Pb^{2+}-3-MPA complex generates defects on the QDs surface which result in PL quenching. Moreover, because the amount of ligand at the QDs surface decreases, QDs may also coalesce which also conducts to a PL quenching.

The Pb^{2+}-3-MPA complex was prepared by reacting $Pb(NO_3)_2$ with 2 equivalents of 3-MPA [66]. As can be seen on Fig. S11, the UV-visible absorption of the Pb^{2+}-3-MPA complex overlaps the PL emission of ZnSeS/Cu:ZnS/ZnS QDs. An energy transfer between the QDs in the excited state and the Pb^{2+}-3-MPA complex in the ground state may occur and be responsible of the PL quenching observed. The dipole-dipole interactions between the QDs and the quencher involved in the energy transfer mechanism may also explain why ZnSeS/Cu:ZnS/ZnS QDs were found to be the most efficient for detecting Pb^{2+} compared to ZnSeS/Cu:ZnS QDs in which the distance between the photoluminescent centers and the quencher is smaller (see Fig. S6).

Based on UV-visible absorption and PL lifetime measurements, the following dynamic quenching mechanism can be proposed. ZnSeS/Cu:ZnS/ZnS QDs are well dispersed in aqueous solution due to the high density of the 3-MPA ligand at their surface (Zeta potential of -76 mV). Upon addition of Pb^{2+}, collision interaction between ZnSeS/Cu:ZnS/ZnS QDs and Pb^{2+} ions occurs. The partial displacement of the 3-MPA ligand from the QDs surface changes the surface properties and generates defects that may be responsible of the PL quenching. Simultaneously, an energy transfer between ZnSeS/Cu:ZnS/ZnS QDs in their excited state and the Pb^{2+}-3-MPA complex may also be involved in the PL quenching.

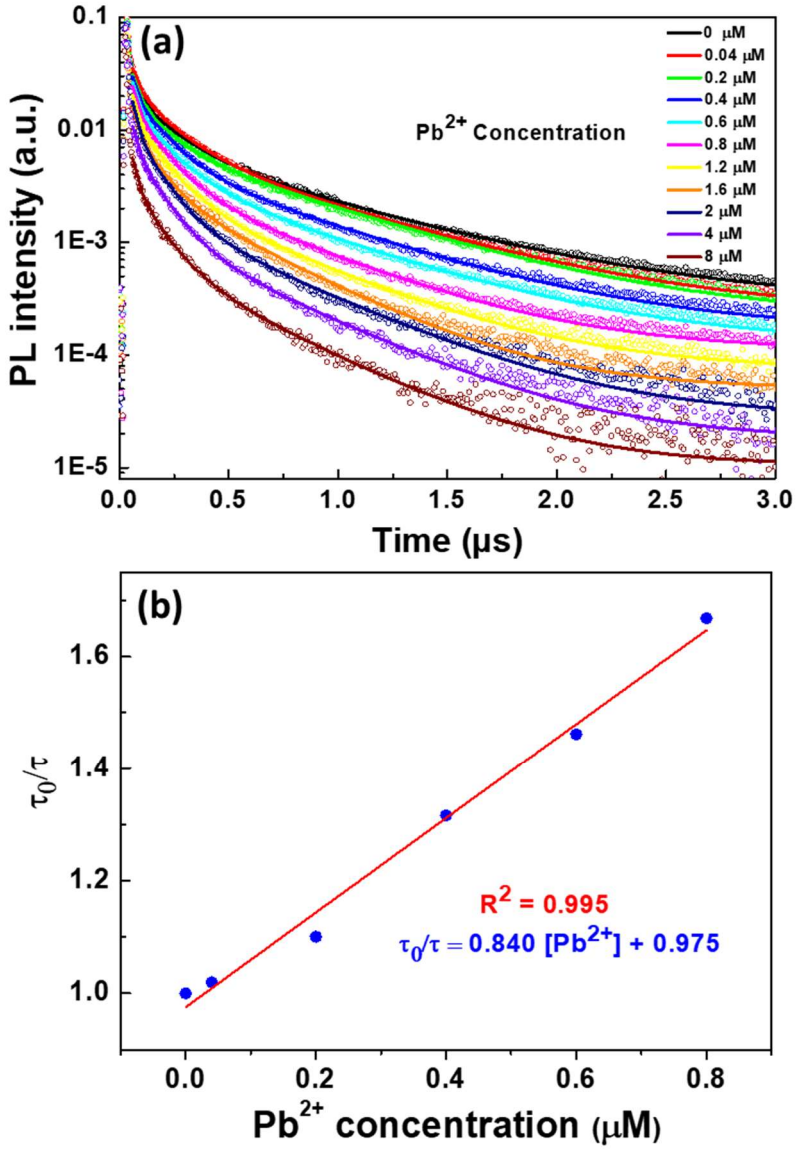

Fig. 8. (a) Effect of the Pb^{2+} concentration on the PL lifetime of ZnSeS/Cu:ZnS/ZnS QDs. (b) Stern-Volmer plot of the PL lifetime vs the Pb^{2+} concentration.

Table 1. Fluorescence decay parameters as a function of the Pb^{2+} concentration.

$[Pb^{2+}]$ (μM)	A_1	τ_1 (μs)	A_2	τ_2 (μs)	A_3	τ_3 (μs)	τ_{av} (μs)
0	0.023	0.033	0.014	0.165	0.007	0.746	0.189
0.04	0.023	0.031	0.017	0.169	0.007	0.698	0.182
0.2	0.029	0.028	0.015	0.133	0.007	0.669	0.154
0.4	0.020	0.023	0.016	0.134	0.005	0.638	0.145
0.6	0.024	0.027	0.013	0.145	0.004	0.633	0.125

0.8	0.020	0.022	0.014	0.123	0.003	0.533	0.109
1.2	0.015	0.023	0.011	0.126	0.003	0.518	0.113
1.6	0.012	0.022	0.008	0.102	0.003	0.431	0.108
2	0.013	0.020	0.009	0.110	0.002	0.497	0.094
4	0.008	0.021	0.006	0.110	0.001	0.477	0.096
8	0.006	0.024	0.003	0.109	7.872E-4	0.439	0.084

4. Conclusion

3-Mercaptopropionic acid capped core/shell/shell ZnSeS/Cu:ZnS/ZnS QDs with an average diameter of ca. 1.8 nm were prepared via a facile and one-pot aqueous method. The Cu-related PL emission of ZnSeS/Cu:ZnS/ZnS nanocrystals is located at 500 nm and their PL QY is of 21%. A marked quenching of the QDs PL was observed with the increase of the Pb^{2+} ions concentration and a dynamic quenching mechanism was demonstrated based on UV-visible absorption and PL lifetime measurements. The results show that ZnSeS/Cu:ZnS/ZnS QDs can selectively sense Pb^{2+} ions in ultrapure water and in real water samples. The limits of detection are 21, 76 and 28 nM in ultrapure water, mineral water and lake water, respectively. The fast response and the high sensitivity of ZnSeS/Cu:ZnS/ZnS QDs towards Pb^{2+} combined with the low interference effect of other metal cations and biomolecules make these photoluminescent probes of high interest for Pb^{2+} sensing in the environment.

CRediT authorship contribution statement

Salima Mabrouk: Methodology, Investigation, Data curation, Writing – original draft. **Hervé Rinnert**: Investigation, Data curation, Writing – original draft. **Lavinia Balan**: Investigation, Data curation, Writing – original draft. **Jordan Jasniewski**: Investigation, Data curation, Writing – original draft. **Ghouti Medjahdi**: Methodology, Investigation, Data curation. **Rafik Ben Chaabane**: Supervision, Funding acquisition. **Raphaël Schneider**: Supervision, Conceptualization, Writing – review & editing, Funding acquisition.

Declaration of Competing Interest

The authors declare that they have no known competing financial interests or personal relationships that could have appeared to influence the work reported in this paper.

Acknowledgements

This project has benefited from the expertise and the facilities of the Platform MACLE-CVL which was co-funded by the European Union and Centre-Val de Loire Region (FEDER).

Appendix A. Supplementary data

Supplementary data to this article can be found online at https://doi.org/

References

[1] A.L. Wani, A. Ara, J.A. Usmani, Lead toxicity: a review, Interdiscip. Toxicol. 8 (2015) 55-64.

[2] E.S. Ravipati, N.N. Mahajan, S. Sharma, K.V. Hatware, K. Patil, The toxicological effects of lead and its analytical trends: an update from 2000 to 2018, Crit. Rev. Anal. Chem. 51 (2021) 87-102.

[3] A. Kumar, A. Kumar, C.-P. M.M.S., A.K. Chaturvedi, A.A. Shabnam, G. Subrahmanyam, R. Mondal, D.K. Gupta, S.K. Malyan, S.S. Kumar, S.A. Khan, K.K. Yadav, Lead Toxicity: Health Hazards, Influence on Food Chain, and Sustainable Remediation Approaches. Int. J. Environ. Res. Public Health 17 (2020) 2179.

[4] K. Renua, R. Chakrabortya, H. Myakala, R. Kotia, A.C. Famurewa, H. Madhyastha, B. Vellingiri, A. George, A.V. Gopalakrishnana, Molecular mechanism of heavy metals (Lead, Chromium, Arsenic, Mercury, Nickel and Cadmium) - induced hepatotoxicity – A review, Chemosphere 271 (2021) 129735.

[5] R.E. Neuhauser, U. Panne, R. Niessner, G.A. Petrucci, P. Cavalli, N. Omenetto, On-line and in-situ detection of lead aerosols by plasma-spectroscopy and laser-excited atomic fluorescence spectroscopy, Analytica Chimica Acta 346 (1997) 37-48.

[6] J. Sardans, F. Montes, J. Peñuelas, Determination of As, Cd, Cu, Hg and Pb in biological samples by modern electrothermal atomic absorption spectrometry, Spectrochimica Acta Part B 65 (2010) 97–112.

[7] Q. Hu, G. Yang, Y. Zhao, J. Yin, HPLC Determination of copper, nickel, cobalt, silver, lead, cadmium, and mercury ions in water by solid-phase extraction and the RP-HPLC with UV-Vis detection, Anal. Bioanal. Chem. 375 (2003) 831–835.

[8] N. Ruecha, N. Rodthongkum, D.M. Cate, J. Volckens, O. Chailapakule, C.S. Henry, Sensitive electrochemical sensor using a graphene–polyaniline nanocomposite for simultaneous detection of Zn(II), Cd(II), and Pb(II), Anal. Chim. Acta 874 (2015) 40-48.

[9] Q. He, E.W. Miller, A.P. Wong, C.J. Chang, A Selective Fluorescent Sensor for Detecting Lead in Living Cells, J. Am. Chem. Soc. 128 (2006) 9316–9317.

[10] X. Li, G. Wang, X Ding, Y. Chen, Y. Gou, Y. Lu, A "turn-on" fluorescent sensor for detection of Pb^{2+} based on graphene oxide and G-quadruplex DNA, Phys. Chem. Chem. Phys. 15 (2013) 12800-12804.

[11] T. Anand, G. Sivaraman, A. Mahesh, D. Chellappa, Aminoquinoline based highly sensitive fluorescent sensor for lead(II) and aluminum(III) and its application in live cell imaging, Anal. Chim. Acta 853 (2015) 596-601.

[12] D. Bera, L. Qian, T.-K. Tseng, P.H. Holloway, Quantum Dots and Their Multimodal Applications: A Review, Materials 3 (2010) 2260-2345.

[13] S. Kargozar, S. Javad Hoseini, P. Brouki Milan, S. Hooshmand, H.-W. Kim, M. Mozafari, Quantum Dots: A Review from Concept to Clinic, Biotechnol. J. 15 (2020) 2000117.

[14] E. Petryayeva, W. Russ Algar, I.L. Medintz, Quantum Dots in Bioanalysis: A Review of Applications Across Various Platforms for Fluorescence Spectroscopy and Imaging, Appl. Spectroscopy 67 (2013) 215-252.

[15] R.K. Ratnesh, M. Singh Mehata, Investigation of biocompatible and protein sensitive highly luminescent quantum dots/nanocrystals of CdSe, CdSe/ZnS and CdSe/CdS, Spectrochim. Acta A 179 (2017) 201-210.

[16] W. Zhong, C. Zhang, Q. Gao, H. Li, Highly sensitive detection of lead(II) ion using multicolor CdTe quantum dots, Microchim. Acta 176 (2012) 101-107.

[17] E.M. Ali, Y. Zheng, H.-h. Yu, J.Y. Ying, Ultrasensitive Pb^{2+} Detection by Glutathione-Capped Quantum Dots, Anal. Chem. 79 (2007) 9452-9458.

[18] X. Wang, X. Guo, Ultrasensitive Pb^{2+} detection based on fluorescence resonance energy transfer (FRET) between quantum dots and gold nanoparticles, Analyst 134 (2009) 1348-1354.

[19] H. Zhu, T. Yu, H. Xu, K. Zhang, H. Jiang, Z. Zhang, Z. Wang, S. Wang, Fluorescent Nanohybrid of Gold nanoclusters and Quantum Dots for Visual Determination of Lead Ions, ACS Appl. Mater. Interfaces 6 (2014) 21461-21467.

[20] M. Algarra, B.B. Campos, B. Alonso, M.S. Miranda, A.M. Martinez, C.M. Casado, J.C.G. Esteves da Silva, Talanta 88 (2012) 403-407.

[21] Q. Zhao, X. Rong, H. Ma, G. Tao, Dithizone functionalized CdSe/CdS quantum dots as turn-on fluorescent probe for ultrasensitive detection of lead ion, J. Hazard. Mater. 250-251 (2013) 45-52.

[22] Z. Cai, B. Shi, L. Zhao, M. Ma, Ultrasensitive and rapid lead sensing in water based on environmental friendly and high luminescent L-glutathione-capped ZnSe quantum dots, Spectrochim. Acta A 97 (2012) 909-914.

[23] J. Chen, Y. Zhu, Y. Zhang, Glutathione-capped Mn-doped ZnS quantum dots as a room-temperature phosphorescence sensor for the detection of Pb^{2+} ions, Spectrochim. Acta A 164 (2016) 98-102.

[24] T. Gan, N. Zhao, G. Yin, M. Tu, J. Liu, W. Liu, Mercaptopropionic acid-capped Mn-doped ZnS quantum dots as a probe for selective room-temperature phosphorescence detection of Pb^{2+} in water, New J. Chem. 41 (2017) 13425-13434.

[25] V. Sharma, M. Singh Mehata, Synthesis of photoactivated highly fluorescent Mn^{2+}-doped ZnSe quantum dots as affective lead sensor in drinking water, Mater. Res. Bull. 134 (2021) 111121.

[26] S. Bian, C. Shen, H. Hua, L. Zhou, H. Zhu, F. Xi, J. Liu, X. Dong, One-pot synthesis of sulfur-doped graphene quantum dots as a novel fluorescent probe for highly selective and sensitive detection of lead(II), RSC Adv. 6 (2016) 69977-69983.

[27] W. Li, X. Hu, Q. Li, Y. Shi, X. Zhai, Y. Xu, Z. Li, X. Huang, X. Wang, J. Shi, X. Zou, S. Kang, Copper nanoclusters@nitrogen-doped carbon quantum dots-based ratiometric fluorescence probe for lead(II) ions detection in porphyra, Food Chem. 320 (2020) 126623.

[28] X. Niu, Y. Zhong, R. Chen, F. Wang, Y. Liu, D. Luo, A « turn-on » fluorescence sensor for Pb^{2+} detection based on graphene quantum dots and gold nanoparticles, Sens. Actuators B Chem. 255 (2018) 1577-1581.

[29] L. Li, D. Liu, A. Shi, T. You, Simultaneous stripping determination of cadmium and lead ions based on N-doped carbon quantum dots-graphene oxide hybrid, Sens. Actuators B Chem. 255 (2018) 1762-1770.

[30] P. Sharma, M. Singh Mehata, Rapid sensing of lead metal ions in an aqueous medium by MoS_2 quantum dots fluorescence turn-off, Mater. Res. Bull. 131 (2020) 110978.

[31] Z. Golsanamlou, J. Soleymani, S. Abbaspour, M. Siahi-Shadbad, E. Rahimpour, A. Jouyban, Sensing and bioimaging of lead ions in intracellular cancer cells and biomedical media using

amine-functionalized silicon quantum dots fluorescent probe, Spectrochim. Acta A 256 (2021) 119747.

[32] N.S. Karan, D.D. Sarma, R.M. Kadam, N. Pradham, Doping Transition Metal (Mn or Cu) Ions in Semiconductor Nanocrystals, J. Phys. Chem. Lett. 1 (2010) 2863-2866.

[33] D.J. Norris, A.L. Efros, S.C. Erwin, Doped Nanocrystals, Science 319 (2008) 1776-1779.

[10] P. Wu, X.-P. Yan, Doped quantum dots for chemo/biosensing and bioimaging, Chem. Soc. Rev. 42 (2013) 5489-5521.

[34] M. Makkar, R. Viswanatha, Frontier challenges in doping quantum dots: synthesis and characterization, RSC Adv. 8 (2018) 22103-22112.

[35] S. Jana, B.B. Srivastatva, S. Acharya, P.K. Santra, N.R. Jana, D.D. Sarma, N. Pradhan, Prevetion of photooxidation in blue-green emitting Cu doped ZnSe nanocrsytals, Chem. Commun. 46 (2010) 2853-2855.

[36] S. Gul, J.K. Cooper, C. Corrado, B. Vollbrecht, F. Bridges, J. Guo, J.Z. Zhang, Synthesis, Optical and Structural Properties, and Charge Carrier Dynamics of Cu-Doped ZnSe Nanocrystals, J. Phys. Chem. C 115 (2011) 43, 20864–20875.

[37] G. Xue, W. Chao, N. Lu, S. Xingguang, Aqueous synthesis of Cu-doped ZnSe quantum dots, J. Lumin. 131 (2011) 1300-1304.

[38] M. Geszke-Moritz, G. Clavier, J. Lulek, R. Schneider, Copper- or manganese-doped ZnS quantum dots as fluorescent probes for detecting folic acid in aqueous media, J. Lumin. 132 (2012) 987-991.

[39] S. Kou, T. Yao, X. Xu, R. Zhu, Q. Zhao, J. Yang, Facile synthesis and optical properties of ultrathin Cu-doped ZnSe nanorods, CrystEngComm 15 (2013) 10495-10499.

[40] H. Labiadh, T. Ben Chaabane, L. Balan, N. Becheik, S. Corbel, G. Medjahdi, R. Schneider, Preparation of Cu-doped ZnS QDs/TiO_2 nanocomposites with high photocatalytic activity, Appl. Catal. B: Environ. 144 (2014) 29-35.

[41] M. Molaei, A.R. Khezripour, M. Karimipour, Synthesis of ZnSe nanocrystals (NCs) using a rapid microwave irradiation method and investigation of the effect of copper (Cu) doping on the optical properties, Appl. Surf. Sci. 317 (2014) 236-240.

[42] S. Gul, J.K. Cooper, P.-A. Glans, J. Guo, V.K. Yachandra, J. Yano, J.Z. Zhang, Effect of Al^{3+} Co-doping on the Dopant Local Structure, Optical Properties, and Exciton Dynamics in Cu^{+}-Doped ZnSe Nanocrystals, ACS Nano 7 (2013) 8680-8692.

[43] J.K. Cooper, S. Gul, S.A. Lindley, J. Yano, J.Z. Zhang, Tunable Photoluminescent Core/Shell Cu^{+}-Doped ZnSe/ZnS Quantum Dots Codoped with Al^{3+}, Ga^{3+}, or In^{3+}, ACS Appl. Mater. Interfaces 7 (2015) 10055-10066.

[44] F. Gong, L. Sun, H. Ruan, H. Cai, Hydrothermal synthesis and photoluminescence properties of Cu-doped ZnSe quantum dots using glutathione as stabilizer, Mater. Express 8 (2018) 173-181.

[45] C. Rajesh, C.V. Phadnis, K.G. Sonawane, S. Mahamuni, Synthesis and optical properties of copper-doped ZnSe quantum dots, Phys. Scr. 90 (2015) 015803.

[46] J.Y. Cui, K.Y. Li, L. Re, J. Zhao, T.D. Shen, Photogenerated carriers enhancement in Cu-doped ZnSe/ZnS/L-cys self-assembled core-shell quantum dots, J. Appl. Phys. 120 (2016) 184302.

[47] K.Y. Li, L.S. Yang, J.Y. Cui, S. Li, G. Li, Effect of doping mechanism on photogenerated carriers behavior in Cu-doped ZnSe/ZnS/L-Cys core-shell quantum dots, AIP Advances 9 (2019) 115021.

[48] Y. Wu, S. Chen, Y. Weng, Y. Zhang, C. Wu, L. Sun, S. Zhang, Q. Yan, T. Guo, X. Zhou, Facile synthesis and color conversion of Cu-doped ZnSe quantum dots in an aqueous solution, J. Mater. Sci. Mater. Electron. 30 (2019) 21406-21415.

[49] H. Qian, X. Qiu, L. Li, J. Ren, Microwave-Assisted Aqueous Synthesis: A Rapid Approach to Prepare Highly Luminescent ZnSe(S) Alloyed Quantum Dots, J. Phys. Chem. B 110 (2006) 9034–9040.

[50] S. Mabrouk, H. Rinnert, L. Balan, S. Blanchard, J. Jasniewski, G. Medjahdi, R. Ben Chaabane, R. Schneider, Aqueous synthesis of highly luminescent ternary alloyed Mn-doped ZnSeS quantum dots capped with 2-mercaptopropionic acid, J. Alloys Compd. 858 (2021) 158315.

[51] O. Adegoke, P. Mashazi, T. Nyokong, P.B.C. Forbes, Fluorescence properties of alloyed ZnSeS quantum dots overcoated with ZnTe and ZnTe/ZnS shells, Opt. Mater. 54 (2016) 104-110.

[52] O. Adegoke, C. McKenzie, N.N. Daeid, Multi-shaped cationic gold nanoparticle-l-cysteine-ZnSeS quantum dots hybrid nanozyme as an intrinsic peroxidase mimic for the rapid colorimetric detection of cocaine, Sens. Actuators B Chem. 287 (2019) 416-427.

[53] J.-Y. Yoo, Y.J. Choi, J.-G. Kim, Synthesis of narrow blue emission gradient ZnSeS quantum dots and their quantum dot light-emitting diode device performance, J. Lumin. 240 (2021) 118415.

[54] R. Zeng, R. Shen, Y. Zhao, Z. Sun, X. Li, J. Zheng, S. Cao, B. Zou, Water-soluble, highly emissive, color-tunable and stable Cu-doped ZnSeS/ZnS core/shell nanocrystals, CrystEngComm 16 (2016) 3414-3423.

[55] L.C. de S. Viol, E. Raphael, J. Bettini, J.L. Ferrari, M.A. Schiavon, A Simple Strategy to Prepare Colloidal Cu-Doped ZnSe(S) Green Emitter Nanocrystals in Aqueous Media, Part. Part. Syst. Charact. 31 (2014) 1084-1090.

[55] F. Gong, L. Sun, H. Ruan, H. Cai, Hydrothermal synthesis and photoluminescence properties of Cu-doped ZnSe quantum dots using glutathione as stabilizer, Mater. Express 8 (2018) 173-181.

[57] J.K. Cooper, S. Gul, S.A. Lindley, J. Yano, J.Z. Zhang, Tunable Photoluminescent Core/Shell Cu^{+}-Doped ZnSe/ZnS Quantum Dots Codoped with Al^{3+}, Ga^{3+}, or In^{3+}, ACS Appl. Mater. Interfaces 7 (2015) 10055-10066.

[58] S. Gul, J.K. Cooper, C. Corrado, B. Vollbrecht, F. Bridges, J. Guo, J.Z. Zhang, Synthesis, Optical and Structural Properties, and Charge Carrier Dynamics of Cu-Doped ZnSe Nanocrystals, J. Phys. Chem. C 115 (2011) 20864-20875.

[59] Y. Wu, S. Chen, Y. Weng, Y. Zhang, C. Wu, L. Sun, S. Zhang, Q. Yan, T. Guo, X. Zhou, Facile synthesis and color conversion of Cu-doped ZnSe quantum dots in an aqueous solution, J. Mater. Sci.: Mater. Electron. 30 (2019) 21406-21415.

[60] J. Kim, H.S. Choi, A. Wedel, S.-Y. Yoon, J.-H. Jo, H.M. Kim, C.-J. Han, H.-J. Song, J.-M. Yi, J.-S. Jang, H. Zschiesche, B.-J. Lee, K. Park, H. Yang, Highly luminescent near-infrared Cu-doped InP quantum dots with a Zn-Cu-In-S/ZnS double shell scheme, J. Mater. Chem. C 2021, 9, 4330-4337.

[61] F. Zu, F. Yan, Z. Bai, J. Xu, Y. Wang, Y. Huang, X. Zhou, The quenching of the fluorescence of carbon dots: A review on mechanisms and applications, Microchim. Acta 184 (2017) 1899-1914.

[62] M. Li, X. Zhou, S. Guo, N. Wu, Detection of lead(II) with a “turn-on” fluorescent biosensor based on energy transfer from CdSe/ZnS quantum dots to graphene oxide, Biosens. Bioelectron. 43 (2013) 69-74.]

[63] W. Zhang, X; Zhou, X. Zhong, One-Pot Noninjection Synthesis of Cu-Doped $Zn_xCd_{1-x}S$ Nanocrystals with Emission Color Tunable over Entire Visible Spectrum, Inorg. Chem. 51 (2012) 3579-3587.

[64] W. Zhang, Q. Lou, W. Ji, J. Zhao, X. Zhong, Color-Tunable Highly Bright Photoluminescence of Cadmium-Free Cu-Doped Zn–In–S Nanocrystals and Electroluminescence, Chem. Mater. 26 (2014) 1204-1212.

[65] C. Corrado, J.K. Cooper, M. Hawker, J. Hensel, G. Livingston, S. Gul, B. Vollbrecht, F. Bridges, J.Z. Zhang, Synthesis and Characterization of Organically Soluble Cu-Doped ZnS Nanocrystals with Br Co-activator, J. Phys. Chem. C 115 (2011) 14559-14570.

[66] H. Shindo, T.L. Brown, Infrared Spectra of Complexes of L-Cysteine and Related Compounds with Zinc(II), Cadmium(II), Mercury(II) and Lead(II), J. Am. Chem. Soc. 87 (1965) 1904-1906]